JOURNAL OF APPLIED PHYSICS **113**, 064311 (2013)

Interfacial thermal conductance limit and thermal rectification across vertical carbon nanotube/graphene nanoribbon-silicon interfaces

Ajit K. Vallabhaneni,[1] Bo Qiu,[1] Jiuning Hu,[2,3] Yong P. Chen,[2,3,4] Ajit K. Roy,[5] and Xiulin Ruan[1,3,5,a)]

[1]*School of Mechanical Engineering, Purdue University, West Lafayette, Indiana 47907, USA*
[2]*School of Electrical Computer Engineering, Purdue University, West Lafayette, Indiana 47907, USA*
[3]*Birck Nanotechnology Center, Purdue University, West Lafayette, Indiana 47907, USA*
[4]*Department of Physics, Purdue University, West Lafayette, Indiana 47907, USA*
[5]*Materials and Manufacturing Directorate, Air Force Research Laboratory, Wright Patterson Air Force Base, Dayton, Ohio 45433, USA*

(Received 11 August 2012; accepted 21 January 2013; published online 13 February 2013)

Various models were previously used to predict interfacial thermal conductance of vertical carbon nanotube (CNT)-silicon interfaces, but the predicted values were several orders of magnitude off the experimental data. In this work, we show that the CNT filling fraction (the ratio of contact area to the surface area of the substrate) is the key to remedy this discrepancy. Using molecular dynamics, we have identified an upper limit of thermal interface conductance for C-Si interface which is around 1.25 GW/m^{2}K, corresponding to a 100% filling fraction of carbon nanotube or graphene nanoribbon on substrate. By extrapolating to low filling fraction ($\sim$1%) that was measured in experiments, our predicted interfacial thermal conductance agrees with experimental data for vertical CNT arrays grown on silicon substrate ($\sim$3 MW/m^2 K). Meanwhile, thermal rectification of more than 20% has been found at these C-Si interfaces. We observed that this is strongly dependent on the interfacial temperature drop than the filling fraction. This new effect needs to be considered in future thermal interface materials design. [http://dx.doi.org/10.1063/1.4790367]

I. INTRODUCTION

As the size of microelectronic devices shrinks, the ratio of surface area to volume increases and heat transfer at these sub-micron scales is dominated by interfaces, across which air gaps are present leading to poor heat removal. Hence applying thermal interface materials (TIM's) to enhance thermal conductance across the contacts becomes essential.[1–3] A superior TIM should possess high thermal conductivity itself and strong bonding to the substrate. It has been experimentally demonstrated that carbon nanotubes (CNT) and graphene have very high thermal conductivity which makes them promising candidates for TIM.[4] The performance of CNT's has been investigated extensively in the last decade.[5–13] Recently, Tong *et al*. have measured the thermal conductance of a vertical CNT-Si interface to be of the order of 3 MW/m^2 K.[11] They also observed an order of magnitude increase in thermal conductance of CNT-glass interface by bonding the two surfaces using an indium weld highlighting the significance of strong thermal contact at the interface. A similar study by Xu *et al*. on a vertical MWCNT–Cu interface concluded that nanotube alignment, density, and growth conditions affect the overall thermal conductance.[10] Despite encouraging progress, the performance of CNT based thermal interface materials is still far from their potential. This is mainly due to the effective volume fraction of CNT's contributing to thermal conduction (0.5%) being very much less than the growth volume fraction of 12% (which in itself is quite low).[12,13] Therefore, promoting good contact and covalent bonding between CNT and the substrate have been identified as a key to further reduce interfacial resistance, and novel chemical methods have been proposed for this purpose.[14]

Theoretical studies especially molecular dynamics simulations have also been performed to relate the interface thermal resistance of CNT-substrate to their atomic structure. Molecular dynamics is an effective method for this purpose because it does not require any assumptions about phonon scattering rates at the complex interface or prior knowledge of thermal transport of the system from experiments. For instance, the contact resistance between CNT-CNT tips has been modeled using MD, where the inter-tube interactions are assumed to be van der Waals.[15] MD simulations have also been done on CNT-Si interface,[16–18] where the results suggest that the interface resistance is sensitive to factors such as pressure, temperature, number of bonds, and CNT functionalization. However, the predicted interface conductance was orders of magnitude higher than experimental data. The discrepancy, as we will identify, arises from the fact that the effective filling fraction of CNT (fraction of the actual CNT-substrate contact area to the whole substrate area) was not taken into account in the simulations.

Like CNT, graphene nano ribbons (GNRs), narrow strips of graphene with several nanometers in width, have been considered as important elements in future carbon-based nanoelectronics. It has been demonstrated that graphene has very high thermal conductivity[4,19,20] and less thermal boundary resistance in using along with heat sinks.[21] In our previous work, we predicted high thermal conductivity of GNRs using molecular dynamics.[22] Although free-standing graphene flakes have already been grown on

[a)]E-mail: ruan@purdue.edu.

various substrates including silicon,[23] no theoretical or experimental studies have been preformed to evaluate their interfacial thermal conductance.

In this paper, we use non-equilibrium molecular dynamics simulations to investigate the thermal interface conductance as a function of the CNT or GNR filling fraction on the Si substrate, and compare the difference of using CNT and GNR. Based on the information, we identify an upper limit of thermal interface conductance which can be used conveniently to treat any realistic filling fraction of CNT or GNR on substrate. Our predicted results are in very good agreement with the experimental data. We also observe strong thermal rectification across the interface which is an important mechanism to be taken into account for future TIM design.

II. METHODOLOGY

Our system consists of a GNR 10 nm long and 3.2 nm wide placed horizontally against {100} face of silicon block of size $6 \times 6 \times 18$ unit cells (3.26×3.26 nm^2 cross-section) as shown in Figure 1. The atoms at the two ends of the system are fixed (black colored in Figure 1) to avoid any rotation/translation which may result from the velocity scaling, and periodic boundary conditions are applied in the other two directions. We have confirmed that different boundary conditions do not alter our conclusions about the interfacial conductance significantly. The filling fraction of GNR on the substrate is defined as the ratio of contact area (A_c) to cross-sectional area of substrate (A_s). The contact area A_c refers to the total cross-sectional area of GNRs, so varying the number of layers of GNR in the vertical (z) direction varies the contact area, resulting in varying filling fraction. Interlayer distance is maintained at 0.335 nm (same as in graphite) although it is observed that varying the distance does not influence the overall thermal conductance significantly.

A. Density functional theory (DFT)

To understand the nature of bonding at the GNR-silicon interface, we compute the charge distribution in the framework of DFT.[24] Due to the similarity of GNR-Si and CNT-Si bonding, here we only considered an armchair (5,5) CNT which has a small diameter for computational feasibility. So far, there has been very limited knowledge about the interfacial bonding nature between CNT (or GNR) and silicon. Orellana *et al.*[25] and Miwa *et al.*[26] studied the configurations of CNT horizontally lying on top of free or hydrogenated silicon from first principles calculations. They found that the bonding at CNT-silicon interface is a mixture of van der Waals (vdW) and covalent bonds in general. Also, there are only vdW bonds after hydrogenation of silicon surface. However, the bonding nature at a vertical CNT/graphene-silicon interface is not yet clear.

With the local density approximation (LDA), the Ceperley-Alder exchange-correlation functional[27] and Vanderbilt pseudo potential[28] are employed for the calculations using the VASP code.[29] We consider the armchair (5,5) CNT vertically adsorbed on the reconstructed Si(001) surface. The surface is simulated using slab geometry containing five Si monolayers (ML) with 3×3 surface unit cells. The CNT is released at 2.0 Å above the silicon surface. About 10 Å thick vacuum regions are created above the top of CNT and below the bottom Si ML, respectively. Due to the large size of the supercell, only the Γ point was used for Brillouin zone sampling. With the bottom Si ML fixed, the geometry optimization is performed until the force components of all the atoms become smaller than 0.05 eV/Å. The optimized final geometry is shown in Figure 2. There are 10 carbon atoms at the CNT-silicon interface. From the equilibrium structure, we found that all carbon atoms formed bonds with silicon atoms at the interface with bond lengths varying from 1.80 to 2.01 Å. In the left panel of Figure 2, the 0.6 e/Å^3 charge density isosurface shows the formation of very dense bonds between C and Si atoms with charge more bounded to the C atom. In pristine CNT, the C-C bond is formed with sp^2-sp^2 hybridized orbitals, while the Si-Si bond in silicon is formed with sp^3-sp^3 hybridized orbitals. Therefore, the C-Si bond at CNT-silicon interface is likely to be sp^3-sp^2 bond.

Such bond should be a little stronger than but similar to that in SiC which involves one sp^3 hybridized orbital

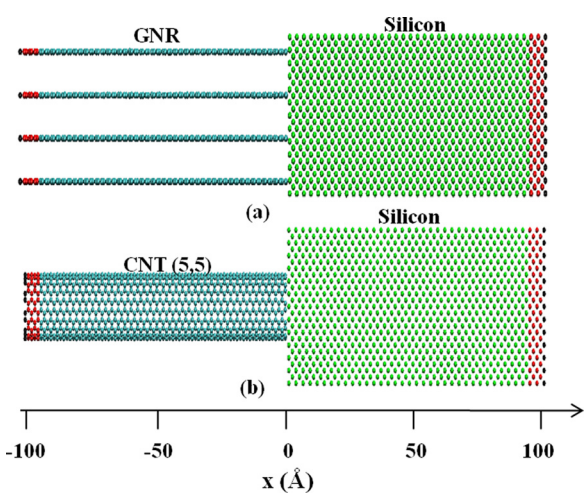

FIG. 1. Typical simulation setup used in the present work: (a) single layer GNR and (b) a SWCNT placed vertically along a silicon substrate. The fixed atoms are denoted by black color, and the thermostated atoms are denoted by red color.

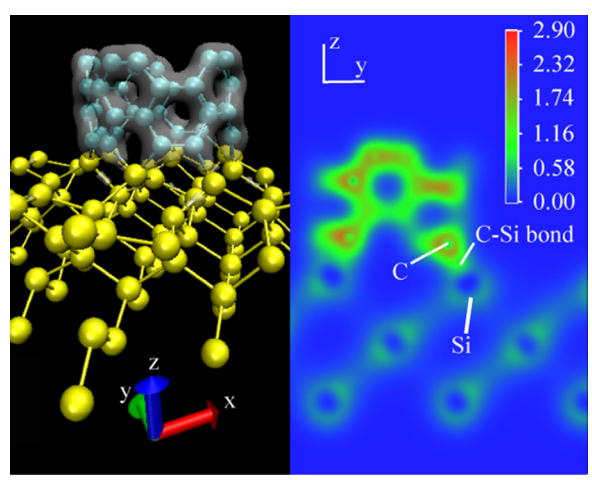

FIG. 2. Charge density plots to visualize the C-Si bonds. Left panel: 0.6 e/Å^3 charge density isosurface plot; Right panel: yz plane 2D charge density plot that goes through C and Si atoms at the interface. The unit of the color scale is e/Å^3.

from both C and Si atoms. This can be verified by comparing the 2D charge density plot that goes through C and Si atoms at the interface (right panel of Figure 2) to that in silicon carbide (not shown).[30] It's found that the bonds at the interface are indeed very similar to that in SiC in both shape and charge density distribution. The averaged C-Si bond length at the interface is 1.897 Å, which is a little longer than the C-Si bond in SiC (1.868 Å from an independent calculation). This is due to the specific coordination of the CNT with respect to silicon surface that some sp^3-sp^2 bonds are stretched. To sum up, for CNT vertically adsorbed on Si (001) surface, all carbon atoms at the interface form covalent bonds that are similar in strength to the bonds in SiC.

B. Molecular dynamics (MD)

After confirming the covalent bond nature of the C-Si interactions, we employed many body Tersoff potential (developed for SiC) to model all the C-C, C-Si, and Si-Si interactions in the system.[31] The interfacial distance has been maintained below the chemical bond length (2.5 Å) of the Tersoff potential. The interlayer interactions of GNR are modeled after Lennard-Jones (LJ) potential with $\varepsilon = 0.00284$ eV and $\sigma = 3.4$ Å. The dynamics of the system are simulated through MD simulations using LAMMPS package.[32] First, the system is equilibrated to 300 K in an NVT ensemble using Nose-Hoover thermostat for 1 ns using a timestep (Δt) of 0.25 fs. Subsequently, the system has been transformed to a micro-canonical (NVE) ensemble where non-equilibrium is introduced in the system.

By adding and removing a known value of heat flux from the two regions adjacent to the fixed ends (shown in red color in Figure 1) simultaneously, temperature gradient has been created in the system. The direction of heat flow when energy is added on the silicon end and removed on the GNR end is denoted by a '+' sign and the opposite direction of heat flow by a '−' sign in the text that follows. This method is preferred to the other methods as we observed that the algorithm used in the velocity scaling conserves the velocity of the center of mass of thermostat. It is also free of any artifacts and offers stability over the rest with respect to the simulation parameters like timestep. The temperatures in the regions of heat addition/removal are controlled by scaling the velocities of atoms using the algorithm described by Jund and Jullien.[33]

$$v_{i,new} = v_{i,old} \pm \alpha\,(v_{i,old} - v_{cm}). \tag{1}$$

Here, $v_{i,old}$, $v_{i,new}$ are the velocities of the atoms before and after scaling, respectively, v_{cm} is the velocity of the center of mass before rescaling and α is the scaling factor given by

$$\alpha = \sqrt{1 \pm \frac{\Delta\varepsilon}{\varepsilon_R}}, \tag{2}$$

where $\Delta\varepsilon$ is the amount of heat added or removed at each time step and ε_R is the relative kinetic energy of the section. The magnitude of heat flux (J_F) is obtained by

$$J_F = \frac{\Delta\varepsilon}{A\Delta t}, \tag{3}$$

where A represents the area of cross-section normal to the direction of the heat flow and Δt is the timestep. The total energy of the system remains unchanged since equal amounts of energy is added and removed simultaneously at each timestep. The simulation domain is divided into bins of approximately 5 Å thickness along the direction of heat flow. By calculating the temperatures of individual bins and averaging them over the last 1 ns of the simulation time, the final steady state temperature profiles are obtained. The entire simulation run time is approximately 9 ns, which is enough for the system to reach the steady state. Repeating the simulation over a longer time did not change the temperature profile and thereby the thermal conductance. Thereafter, the signs of the heat flux on both the ends are interchanged and similar procedure is repeated to extract the temperature profile.

III. RESULTS AND DISCUSSION

The sample steady state temperature profiles for a six layer GNR—Si interface in both directions of heat flow are plotted in Figure 3. A drop in temperature (ΔT) is observed across the interface because of the thermal boundary resistance. It can be observed that the temperature drops in both directions of heat flow are different. This is an indication of thermal rectification phenomenon which has been observed in various structures with geometrical[22] and material[34] asymmetry. The thermal conductance per unit cross-sectional area of the substrate (G_s) is calculated as:

$$G_s = \frac{J}{A_s \Delta T} = \frac{J}{A_c \Delta T}\left(\frac{A_c}{A_s}\right) = G_c\left(\frac{A_c}{A_s}\right), \tag{4}$$

where J is the heat current, A_s is the cross-sectional area of the substrate, and A_c is the contact area defined as the product of the width (w) and thickness (t) of single layer GNR

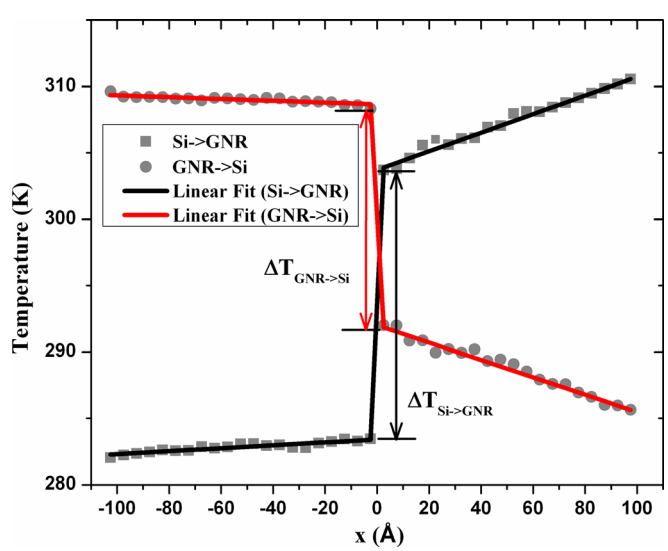

FIG. 3. Steady state temperature profiles of a 6-layer GNR on silicon substrate for J = 0.15 μW.

which is equal to 0.335 nm. Here, G_c is defined as the normalized thermal conductance or the thermal conductance per unit contact area, and it represents the upper bound of G_s, in principle achievable at a 100% filling fraction A_c/A_s.

It is evident that G_s increases with the filling fraction A_c/A_s since it enables more C-Si bonds at the interface and thereby providing more channels for heat flow. Figure 4(a) shows G_s as a function of A_c/A_s for GNR/CNT-Si interface in both directions of heat flow for a constant value of J = 80 nW. Within the range of filling fraction that we have simulated (from 6% to 83%), G_s varies almost linearly with A_c/A_s, indicating that G_c approximately remains constant without being sensitive to A_c/A_s. For filling fraction of 6.7%, the thermal conductance is 57 MW/m^{2}K when heat flows from Si to GNR. In experiments, a growth fraction of 10% of CNT can be achieved. However, it has been pointed out that probably only 1% of CNT is in real contact with substrate while the other 9% do not actually contribute to heat transfer.[13] Simulating a 1% filling fraction is numerically unstable, but when linearly extrapolating our results to 1%, as shown in the inset of Figure 4(a), we obtain $G_s = 8$ MW/m^{2}K which agrees with the experimental data quite well.[5] In previous simulations, the predicted thermal conductance is several orders of magnitude higher than the experimental data because the role of filling fraction was not taken into account.[16,17] Also, the thermal conductance is higher when heat flow is from GNR (or CNT) to silicon when compared to that in the opposite direction.

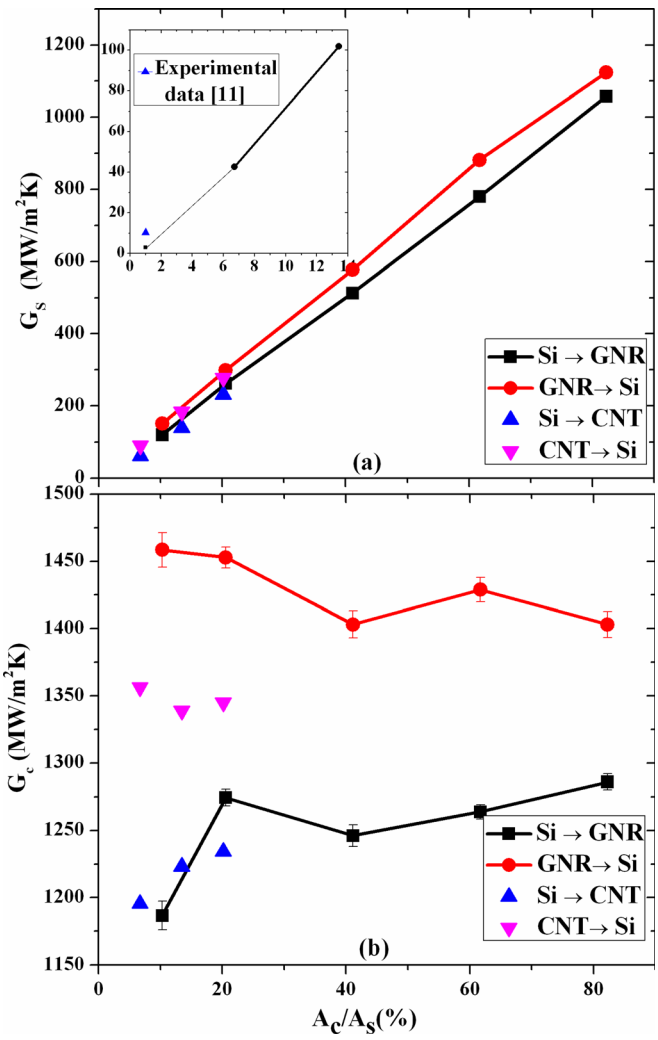

FIG. 4. (a) Variation of thermal conductance with respect to substrate area, G_s and (b) thermal conductance with respect to contact area, G_c as a function of filling fraction (A_c/A_s).

The normalized thermal conductance is plotted in Figure 4(b) which reveals an important aspect of this paper. It can be observed that as the filling fraction increases, G_c reaches a constant value in both directions of heat flow emphasizing the dominance of interfacial resistance over the inter-layer resistance. These normalized values of thermal conductance can be used to estimate the thermal conductance for any particular value of filling fraction using Eq. (4). We also observed that the interlayer distance between GNR layers does not affect the overall thermal conductance. This could be because of the weak van der Waals interactions between the layers. The error bars are obtained by averaging the values of thermal conductance over three independent simulations. As can be noticed from Figure 4, the thermal conductance for GNR and CNT is almost of the same order of magnitude. It implies that the GNR can work on par with CNT's in its application as a TIM. Also, GNR is probably advantageous in achieving higher filling fraction due to its flat planar structure in contrast to the CNT's hollow cylindrical structure. Accordingly, the maximum filling fraction for SWCNT bundles decreases with the diameter. However, using MWCNTs alleviate this problem to an extent by offering more number of bonds at the interface for the same outer wall CNT contact area provided the inner wall CNTs are in perfect contact with Si at the interface. The maximum possible filling fractions along with the corresponding thermal conductance in the GNR/CNT-Si direction are shown in Table I.

We also examined the variation in thermal conductance when the interfacial bonding changes from covalent to van der Waals, since we believe that the bonding at the interface in experiments is a mix of covalent and van der Waals interactions because of the variable lengths of CNT's in the array. So, we increased the distance across the interface beyond the cutoff of tersoff potential and modeled the non-bonded van der Waals interactions between C and Si atoms using Lennard-Jones potential. This leads to a decrease of thermal conductance by 65% emphasizing the need to provide strong thermal contact at the interface.

TABLE I. The maximum possible filling fraction and interfacial thermal conductance (G_c) for different filler materials.

Material	Maximum filling fraction (%)	Thermal conductance G_c (MW/m^{2}K)
GNR	90	1230.2
(5,5) SWCNT	60.3	802.01
(10,10) SWCNT	26.8	357.21
(15,15) SWCNT	20.1	267.33
(10,10)-(15,15) DWCNT	20.1	445.55
(5,5)-(10,10)-(15,15) TWCNT	20.1	534.66

Finally, we would like to comment on the thermal rectification properties exhibited by the interface. As can be noticed in Figure 4, the thermal conductance is not identical in both directions of the heat flow, indicating thermal rectification. The rectification factor ($\eta = (G_- - G_+)/G_+$) calculated for lowest filling fraction for a constant J = 80.1 nW is approximately 23% and gradually approaches near 8% as the filling fraction increases as demonstrated in Figure 5(a). The variation of the average temperature drop (ΔT) is also shown on the axis on the right side. It can be observed that for a constant heat current (J), as the filling fraction increases, both η and ΔT decreases. Please note that the ΔT plotted is the average of the temperature drop in both the directions of heat flow. Figure 5(b) shows the variation of the η as a function of increasing heat current for a constant filling fraction of 20%. As J increases, the temperature drop ΔT increases resulting in the increase of the rectification factor. It can be observed that the value of $\eta = 24\%$ in both the plots correspond to the same value of ΔT even though the filling fractions are different indicating the importance of ΔT in controlling thermal rectification than the filling fraction. Previously, this behavior is explained based on the mismatch in the overlap of the phonon spectra of atoms at the interface on different systems; but we did not observe a significant difference in the overlap of phonon spectra. Similar observation was reported in a recent paper on GGNR interfaces.[35]

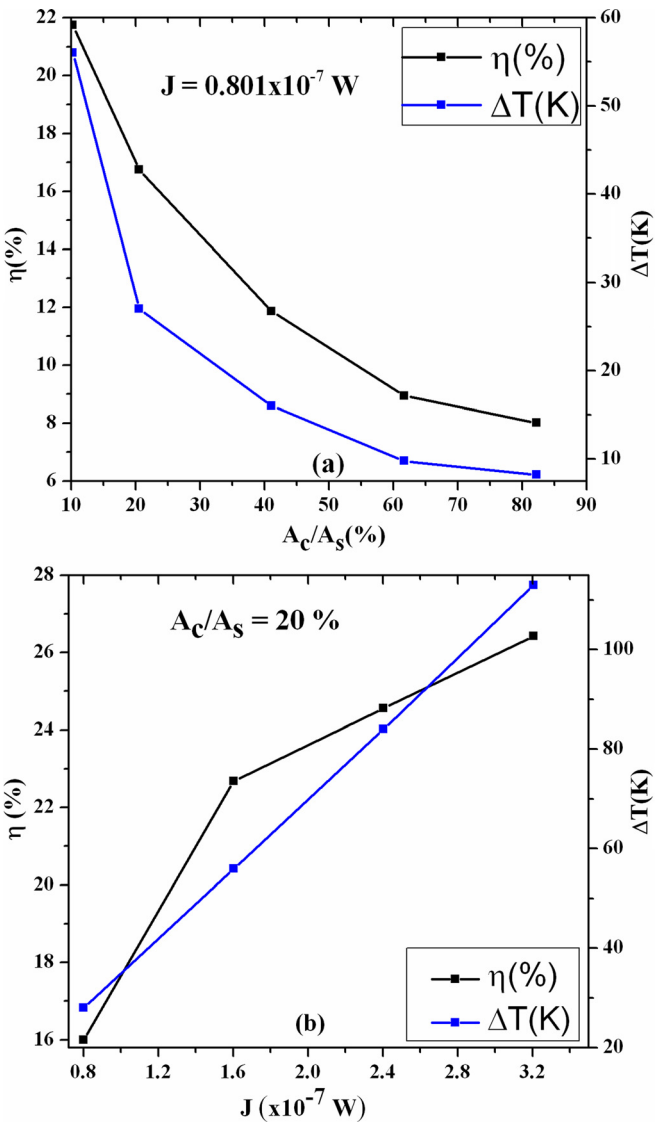

FIG. 5. (a) Thermal rectification factor (η) and temperature drop (ΔT) as a function of filling fraction (A_c/A_s). (b) Thermal rectification factor (η) and temperature drop (ΔT) as a function of heat current (J).

IV. CONCLUSIONS

In summary, we used MD simulations to calculate thermal conductance of GNR-Si and CNT-Si interfaces as a function of filling fraction. We justified the use of SiC potential for modeling the C-Si interactions at the interface using DFT analysis. Our results show that the thermal conductance increases almost linearly with the filling fraction, and we have identified an upper limit of thermal interface conductance of C-Si system The obtained values after taking into account of filling fraction agree with experimental data well emphasizing the fact that high quality thermal contacts are needed to enhance the efficiency of TIM. We also predict significant thermal rectification behavior across these thermal interfaces with the rectification factor being around 20% and emphasized the importance of ΔT in controlling it.

ACKNOWLEDGMENTS

This work was partially supported by the United States Air Force Office of Scientific Research (Grant No.r FA9550-11-1-0057, Program manager Dr. Kumar Jata) and the Cooling Technology Research Center (CTRC). X. L. Ruan also acknowledges the support of Air Force Summer Faculty Fellowship.

[1]R. Prasher, Proc. IEEE **94**, 1571 (2006).
[2]J. P. Gwinn and R. L. Webb, Microelectron. J. **34**, 215 (2003).
[3]A. K. Roy, B. L. Farmer, S. Sihn, V. Varshney, S. Patnaik, and S. Ganguli, Diamond Relat. Mater. **19**, 268 (2010).
[4]A. A. Balandin, S. Ghosh, W. Bao, I. Calizo, D. Teweldebrhan, F. Miao, and C. N. Lau, Nano Lett. **8**, 902 (2008).
[5]J. Xu and T. S. Fisher, Int. J. Heat Mass Transfer **49**, 1658 (2006).
[6]J. Xu and T. S. Fisher, IEEE Trans. Compon. Packag. Technol. **29**, 261 (2006).
[7]X. J. Hu, A. A. Padilla, J. Xu, T. S. Fisher, and K. E. Goodson, J. Heat Transfer **128**, 1109 (2006).
[8]B. A. Cola, J. Xu, C. Cheng, X. Xu, T. S. Fisher, and H. Hu, J. Appl. Phys. **101**, 054313 (2007).
[9]B. A. Cola, X. Xu, and T. S. Fisher, Appl. Phys. Lett. **90**, 093513 (2007).
[10]W. Lin, R. Zhang, K. S. Moon, and C. Wong, Carbon **48**, 107 (2010).
[11]T. Tong, Y. Zhao, L. Delzeit, A. Kashani, M. Meyyappan, and A. Majumdar, IEEE Trans. Compon. Packag. Technol. **30**, 92 (2007).
[12]M. A. Panzer, G. Zhang, D. Mann, X. Hu, E. Pop, H. Dai, and K. E. Goodson, J. Heat Transfer **130**, 052401 (2008).
[13]M. A. Panzer, H. M. Duong, J. Okawa, J. Shiomi, B. L. Wardle, S. Maruyama, and K. E. Goodson, Nano Lett. **10**, 2395 (2010).
[14]W. Lin, R. W. Zhang, K. S. Moon, and C. P. Wong, Carbon **48**, 107 (2010).
[15]H. L. Zhong and J. R. Lukes, Phys. Rev. B **74**, 125403 (2006).
[16]J. Diao, D. Srivastava, and M. Menon, J. Chem. Phys. **128**, 164708 (2008).
[17]M. Hu, P. Keblinski, J. S. Wang, and N. Raravikar, J. Appl. Phys. **104**, 083503 (2008).
[18]H. B. Fan, K. Zhang, and M. M. F. Yuen, J. Appl. Phys. **106**, 034307 (2009).
[19]W. Cai, A. L. Moore, Yanwu Zhu, Xuesong Li, Shanshan Chen, Li Shi, and Rodney S. Ruoff, Nano Lett. **10**, 1645 (2010).
[20]J. H. Seol, Science **328**, 213 (2010).

[21]S. Ghosh, I. Calizo, D. Teweldebrhan, E. P. Pokatilov, D. L. Nika, A. A. Balandin, W. Bao, F. Miao, and C. N. Lau, Appl. Phys. Lett. **92**, 151911 (2008).
[22]J. N. Hu, X. L. Ruan, and Y. P. Chen, Nano Lett. **9**, 2730 (2009).
[23]A. Malesevic, R. Vitchev, K. Schouteden, A. Volodin, L. Zhang, G. Van Tendeloo, A. Vanhulsel, and C. Van Haesendonck, Nanotechnology **19**, 305604 (2008).
[24]W. Kohn, Rev. Mod. Phys. **71**, 1253 (1999).
[25]W. Orellana, Appl. Phys. Lett. **92**, 093109 (2008).
[26]R. H. Miwa, W. Orellana, and A. Fazzio, Appl. Surf. Sci. **244**, 124 (2005).
[27]D. M. Ceperley and B. J. Alder, Phys. Rev. Lett. **45**, 566 (1980).
[28]D. Vanderbilt, Phys. Rev. B **41**, 7892 (1990).
[29]G. Kresse and J. Furthmuller, J. Comput. Mater. Sci. **6**, 15 (1996).
[30]C. H. Park, B. H. Cheong, K. H. Lee, and K. J. Chang, Phys. Rev. B **49**, 4485 (1994).
[31]J. Tersoff, Phys. Rev. B **39**, 5566 (1989).
[32]S. Plimpton, J. Comput. Phys. **117**, 1 (1995).
[33]Z. Huang and Z. Tang, Physica B **373**, 291 (2006).
[34]G. Wu and B. Li, Phys. Rev. B **76**, 085424 (2007).
[35]A. Rajabpour, S. M. V. Allaei, and F. Kowsary, Appl. Phys. Lett. **99**, 051917 (2011).